JOURNAL OF COMPUTATIONAL PHYSICS 95, 1–28 (1991)

Distribution of Event Times in Time-Resolved Fluorescence: The Exponential Series Approach—Algorithm, Regularization, Analysis*

GERHARD LANDL

Institut für Physikalische Chemie, Universität Wien, Währingerstraße 42, A-1090 Wien, Austria

THOMAS LANGTHALER

Institut für Physikalische Chemie, Universität Wien, Währingerstraße 42, A-1090 Wien, Austria and Institut für Mathematik, Johannes-Kepler-Universität, A-4040 Linz, Austria

HEINZ W. ENGL†

Institut für Mathematik, Johannes-Kepler-Universität, A-4040 Linz, Austria

AND

HARALD F. KAUFFMANN†

Institut für Physikalische Chemie, Universität Wien, Währingerstraße 42, A-1090 Wien, Austria

Received June 26, 1989; revised February 8, 1990

In time-resolved fluorescence spectroscopy, a distribution of fluorescence lifetimes resulting from static and dynamic disorder of a polychromophoric ensemble is to be determined from the molecular fluorescence response to the optical probe pulse. To do this, one has to solve a convolution integral equation of the first kind and then invert a Laplace transform. Both problems are ill-posed in the sense of Hadamard. We describe in detail an algorithm that combines coarse discretization for inverting the Laplace transform with a nonlinear least-squares approach based on Newton and quasi-Newton techniques for solving the convolution equation. While this algorithm works well in many cases, it does not completely remove the instabilities due to the ill-posedness. Thus, we also propose an algorithm that combines the approach described above with Tikhonov regularization. Several examples, both with synthetic and with real data, show the performance of our algorithms.

* Supported by the Austrian Fonds zur Förderung der wissenschaftlichen Forschung, projects P6101, P7182, and S32/03.

† Authors to whom correspondence should be addressed.

0021-9991/91 $3.00

1. INTRODUCTION

Over the last decade, time-resolved fluorescence spectroscopy has become a powerful kinetic tool for studying dynamical processes in molecular systems. Chromophores, electronically excited by optical pulses, have fluorescence lifetimes generally in the range of a few picoseconds to some tens of nanoseconds, so transient fluorescence measurements can cover a variety of rapid relaxation events in condensed phase. Typical physical processes that have been probed by fluorescence techniques are conformational transitions, orientational relaxation of fluorophores, energy transfer, polar solvation dynamics, and cis–trans isomerization along a torsion coordinate [19]. In addition, transient fluorescence measurements provide direct access to migrational and rotational sampling in polymers [28, 54], to the modes of internal motion in biological materials [12, 48], and to excitation energy transport in polychromophoric ensembles [2, 3]. Various transient configurations can measure such short time-profiles and among these, the detection technique of single-photon timing (SPT) [40, 52] is now the most sensitive one and preferentially used.

Despite the considerable advances in time resolution and data acquisition, the analysis of fluorescence data encounters several serious problems. One difficulty in evaluating transient patterns arises from a purely mathematical point of view: If $f(t)$, $t \geqslant 0$, characterizes the systems molecular fluorescence response to a Dirac δ-function input at $t=0$, then the impulse fluorescence response to any other optical input pulse, $l(t)$ (called the "lamp-function" below), is the one-sided convolution of l with f,

$$h(t) = \int_0^t l(\tau)\, f(t-\tau)\, d\tau. \tag{1.1}$$

The problem with this Volterra integral equation of the first kind is the following:

The frequency-band limited nature of experimental optical pulses produces finite, temporal waveforms, so that the sharp characteristics of the system's fluorescence impulse response, $f(t)$, are smoothed out, partly beyond recognition. This smoothing property of the integral operator in (1.1) is responsible for the ill-posedness of the deconvolution problem (cf. Section 4). In order to reconstruct the fluorescence pattern, $f(t)$, from smooth data, $h(t)$, one has to solve an ill-posed deconvolution problem [9]. The serious numerical difficulty of treating (1.1) (like any other ill-posed problem) stems form the fact that the collected SPT data, $h(t)$, are superimposed by *noise*, thus, in order to stabilize the inverse procedure in (1.1) and obtain useful boundaries for the error in terms of the Poissonian noise level, regularization has to be used (cf. Section 4). Compared to this "best-case" situation (synthetic data + artificial noise), experimental fluorescence data make the problem worse, as, in addition, time-to-amplitude converter nonlinearities, interfering radio frequencies, pulse-to-pulse instabilities, photomultiplier color effects, light-scattering, and so on will systematically contaminate the error levels of Poisson

counting statistics [40, 52]. Although some of the artefacts can be drastically reduced today, e.g., by correction of the color effects in the instrument response function [8, 55, 56], the distortion caused by the experimental noise level is still high enough and impossible to argue away. Systematic trends and structures in real data make deconvolution of raw data therefore hardly tractable.

To circumvent this problem, methods of iterative forward convolution have been devised, that a priori assume a specific functional form for the decay law. Nonlinear least-squares iterative reconvolution based upon the Levenberg–Marquardt algorithm [20] is a wide-spread analysis technique and, in comparision to transform techniques, quite satisfactory for distorted data, at least for simple exponential decays [41]. *Multiexponential* trial functions that represent the δ-pulse solutions to linear kinetic interconversion processes of fluorescent states have been widely used in the past, with the implicit assumption that the best-fit decay parameters are directly related to some specific kinetic quantities of the underlying physical scheme. Typical examples are the biexponential Birks solutions to a reversible donor–excimer pair [6] which have been applied to the analysis of diffusion in statistically averaged, low-molecular two-component systems [7] and to the description of conformal dynamics in bichromophoric compounds [13]. In addition, triple-exponential forms as exact solutions to coupled three-state models have been used in fluorescence reconvolution analysis with the objective to correlate the optimized (ratios of) amplitudes (eigenvectors) and apparent lifetimes (eigenvalues) to the elementary processes of the hypothesized scheme [10, 32].

However, for molecular systems of ever increasing complexity (amorphous solid state of organic glasses, concentrated dye-solutions, synthetic and biological polymers, micelles, molecules adsorbed on surfaces, etc.), the inhomogeneity of fluorescent chromophores must seriously compromise any analysis in terms of discrete sums-of-exponentials, no matter what the quality of the data and the time-scale over which the data can be collected. In this situation, the number of exponentials extracted by free-fit reconvolution of the data profile must be interpreted to be the result of a pure curve parametrization, and thus, to be exclusively a sum-of-exponentials falsification of a typically *distributed* fluorescence pattern [29]. Distribution of event times and, thus, *nonexponentiality* in fluorescence profiles of such systems generally arises from the vast configurational and conformational multiplicity of molecular arrangements which shows up in a pronounced static or dynamical fluctuation with respect to the spatial, energetic, and temporal coordinates of the fluorophores. As a result, the ensemble and configurational average of chromophore fluorescence probes a large number of relaxing excited-state chromophores, which in case of a continuous distribution of individual exponential decays

$$f(t) = \int_0^\infty \Phi(\tau) e^{-t/\tau}\, d\tau \tag{1.2}$$

represents the quasi-Laplace transform (cf. (2.29)–(2.30)) of the underlying lifetime

distribution function Φ in this formalism. A discretization of the integral (1.2) leads to the Ansatz (2.2) for f. Note that although this leads to a sum of exponentials, the motivation is different from assuming a priori that f is a discrete sum of exponentials. Clearly, the dispersion of event times in the fluorescence of a many-body system imposes an additional difficulty in data analysis. By combining (1.1) and (1.2), we obtain

$$h(t) = l(t) * \int_0^\infty \Phi(\tau) e^{-t/\tau}\, d\tau \tag{1.3}$$

with the spectrum of event-times Φ expressed by the inverse quasi-Laplace transform of the fluorescence signal deconvolved by the lamp function. Since both deconvolution and inverting the Laplace transform are ill-posed problems and, furthermore, the fluorescence response and the pulse shape are incomplete representations for experimental data, the reconstruction of the distribution profile is *de facto* impossible. Naturally, a reconvolution technique which hypothesizes a definite distribution in iterative fit-and-compare cycles should yield a better prognosis. However, the drawback of this method is twofold. First, there exists, for the time being, no certainty for the actual distribution of physical event times in realistic chromophore morphologies, and second, even for distribution functions which might be assumed to be reasonable models, closed form solutions to (1.2) can be scarcely found over typical fluorescence time scales. Thus, the use of nonexponential trial functions in nonlinear least-squares reconvolution is of only little importance for the optimization of the input distribution parameters, at least for decay functions f based upon the formulation in (1.2). Nevertheless, nonexponential solutions as obtained from the treatment of microscopic transport master equations in *random* systems have been used in fluorenscence analysis more recently [1, 25, 42, 43], even though the procedure of such tedious data fit has not been reported in detail. In addition, stretched exponentials of the Kohlrausch–Williams–Watts functional form [53]—a paradigm of fractal-like fluorescence [34, 37, 44]—have been examined as test functions in reconvolution [18]; however, evaluation of the distribution via this rather unspecific function is as yet not feasible, since its microscopic origin is still elusive [35, 36].

Very recently, methods that avoid specific nonexponential fitting functions, but rather deconvolute the fluorescence data by an unbiased algorithm have turned out to be very promising. Both the exponential series method (ESM) developed by James and Ware [30] and the maximum entropy mehtod (MEM) [47] modified to fluorescence analysis by Livesey and Brochon [38] have yielded quite satisfactory results in the reconstruction of distributions [31, 46, 50, 51]. In the ESM, (1.2) is approximated by a series of exponentials with fixed lifetimes τ_k (usually equally spaced over the time scale of fluorescence), which allows the corresponding amplitudes to be evaluated from (1.3) by a *linear* least-squares iterative reconvolution. In order to circumvent partly negative amplitudes in the free-parameter optimization, James and Ware [30] restricted these amplitudes to positive values, thus the analysis is restricted to pure decays only. Furthermore, to improve the

convergence and to speed up the search procedure, they modified the program to automatically remove terms from the exponential series when the preexponentials become less than an arbitrarily chosen cutoff [30]. This approach might distort the result if the algorithm at an intermediate step produces a small value of an amplitude whose "true" value is not close to 0. The more recent MEM is a regularization technique where the Shannon–Jaynes entropy [45] is maximized subject to the additional constraint that $\chi^2 = 1$ (cf. (2.10)) [38]. Since MEM is a regularization method, it tends to be less sensitive to noise than ESM and can therefore work with a larger number of exponentials; moreover, there is no need with MEM to apply a cutoff for deleting pre-exponential terms of values close to zero during the reconvolution [38].

The motivation of this paper is based upon our recent studies on excitation energy transport and rotational sampling in the field of polymer physical chemistry [33, 39]. The work to be presented here is concerned with our recent efforts to develop improved numerical data analysis methods, with the future objective being to determine hopping and rotational frequency distributions in static and dynamical polymer morphologies from a set of experimental fluorescence curves.

In this work, a modified ESM algorithm is presented in Section 2. We use a combination of a quasi-Newton method and the Levenberg–Marquardt method in such a way that the algorithm becomes "as stable as possible"; also negative values for the amplitudes are possible. In Section 3 we show that the algorithm works well on both synthetic and real data. However, the inherent instability of the problem to be solved cannot be overcome by any algorithm that does not use regularization. This is shown by synthetic numerical examples in Section 3. In Section 4, we propose an algorithm based on Tikhonov regularization. While ESM and our algorithm in Section 2 should be seen as "reconvolution algorithms," Tikhonov regularization as used in Section 4 can be considered as a "deconvolution algorithm." The numerical examples in Section 5 show clearly that this algorithm improves the reconstruction from noisy data considerably.

2. The Quasi-Newton Approach

As explained in Section 1, we are concerned with solving the first-kind convolution integral equation

$$h(t) = \int_0^t I(\tau)\, f(t-\tau)\, d\tau, \tag{2.1}$$

where h and I are known up to measurement errors and f is the "decay function" to be computed. Motivated by the fact that f is actually a Laplace transform (cf. (1.2)), we approximate f by functions of the type

$$\tilde{f}(t) := \sum_{i=1}^{n} \tilde{a}_i \cdot e^{-t/\tau_i} \tag{2.2}$$

with a given number n of degrees of freedom and given lifetimes τ_i. We want to determine the amplitudes $\tilde{a}_i$ from (2.1), where we assume a priori that the $\tilde{a}_i$ lie in a given interval

$$\tilde{a}_i \in [\alpha_0, +\infty[, \qquad i \in \{1, ..., n\}, \tag{2.3}$$

with $\alpha_0 \leqslant 0$ given. In order to avoid ending up with a constrained optimization problem, we make the substitution

$$\tilde{a}_i =: \alpha_0 + \tilde{\alpha}_i^2, \qquad i \in \{1, ..., n\}; \tag{2.4}$$

the new unknowns $\tilde{\alpha}_i$ may vary in all of $\mathbb{R}$.

To set up the optimization problem from which the $\tilde{\alpha}_i$ are to be determined, we proceed as follows:

The measurement process defines equally spaced channels

$$t_i = i \cdot h, \tag{2.5}$$

where i typically runs form 1 to $i_{\max} = 256$ or $i_{\max} = 512$, where $i_{\max}$ is the number of channels in an SPT-experiment, and h is typically between 0.2 and 0.8 ns. We use the midpoints between the t_i as knots for a trapezoidal rule for approximating the integral in (2.1) at these knots, which gives

$$\int_0^{t_i - h/2} l(\tau) f(t-\tau)\, d\tau \approx \frac{h}{2} \sum_{j=1}^{i-1} \left[l\left(t_j - \frac{h}{2}\right) f(t_i - t_j) + l\left(t_{j+1} - \frac{h}{2}\right) f(t_i - t_j) \right], \qquad i \in \{1, ..., i_{\max}\}. \tag{2.6}$$

However, l is not known at specific points; only the averages

$$\hat{l}_i := \int_{t_{i-1}}^{t_i} l(\tau)\, d\tau + \eta_i, \qquad i \in \{1, ..., i_{\max}\} \tag{2.7}$$

can be measured (with an error η_i). Thus, we use the formula

$$I(t_i, f) := \frac{h}{2} \sum_{j=1}^{i-1} [\hat{l}_j f(t_i - t_j) + \hat{l}_{j+1} f(t_i - t_j)], \qquad i \in \{1, ..., i_{\max}\}. \tag{2.8}$$

Using (2.8), the approximation (2.2), and the fact that also h cannot be measured at specific points but only in the form of mean values

$$\hat{h}_i := \int_{t_{i-1}}^{t_i} h(\tau)\, d\tau + \delta_i, \qquad i \in \{1, ..., i_{\max}\},$$

with errors δ_i, one could try to determine the unknowns $\tilde{\alpha}_i$ by requiring that

$$I(t_i, \tilde{f}) = \hat{h}_i, \qquad i \in \{1, ..., i_{\max}\}, \tag{2.9}$$

where $\tilde{f}$ has the form (2.2). Note that (2.9) is just a system of linear equations for the original unknowns $\tilde{a}_1, ..., \tilde{a}_n$. Moreover, the constraints (2.3) would have to be taken into account. Because of the fact that the number $i_{\max}$ of channels is typically larger than the number n of degrees of freedom and because of the statistical nature of the measurement errors η_i, δ_i, we have to replace (2.9) by a least-squares criterion; we formulate the following unconstrained minimization problem:

Problem 2.1. Determine $\tilde{\alpha}_1, ..., \tilde{\alpha}_n \in \mathbb{R}$ such that

$$\chi^2 := \sum_{i=i_l}^{i_u} w_i (I(t_i, \tilde{f}) - \hat{h}_i)^2 \to \min, \tag{2.10}$$

where $\tilde{f}$ has the form (2.2) and the unknowns $\tilde{\alpha}_1, ..., \tilde{\alpha}_n$ are given by (2.4); see (2.11) and the following discussion for the remaining quantities.

The weights are given by

$$w_i := 1/\hat{h}_i; \tag{2.11}$$

for a statistical motivation see [23]; since this statistical motivation is relevant only for large $\hat{h}_i$ and since $\hat{h}_i$ tends to be small for very small and very large indices i, we sum between two fixed indices i_l and i_u in (2.10) which are chosen such that $\hat{h}_i$ is not too small for $i_l \leqslant i \leqslant i_u$.

Note that so far, the only difference between Problem 2.1 and the usual approach in the literature is the transformation (2.4); e.g., in [29–31], (2.9) is minimized by a Marquardt-type method (cf. [20]) with respect to the original $\tilde{a}_i \geqslant 0$. The constraints are taken into account in such a way that as soon as the algorithm produces a sufficiently small $\tilde{a}_i$, this $\tilde{a}_i$ is put $= 0$, once and forever. This is a quite heuristic approach for dealing with constraints, which could be improved considerably, e.g., by using an active index-set strategy (cf. [21]). However, since the transformation (2.4) removes the constraint anyway, we do not pursue this line. Instead, our approach is based on using a more sophisticated algorithm for the unconstrained optimization of Problem 2.1, which we describe below.

From now on, let

$$\alpha := (\tilde{\alpha}_1, ..., \tilde{\alpha}_n) \tag{2.12}$$

and

$$\begin{aligned} r_i(\alpha) &:= \sqrt{w_i} \cdot (\hat{h}_i - I(t_i, \tilde{f})), \\ r(\alpha) &:= (r_{i_l}(\alpha), ..., r_{i_u}(\alpha)). \end{aligned} \tag{2.13}$$

Then the objective function in (2.10) is just $\|r(\alpha)\|^2$; by $\langle\ ,\ \rangle$ and $\|\ \|$, we denote the usual Euclidean inner product and norm, respectively. Thus, Problem 2.1 now reads

$$\|r(\alpha)\|^2 \to \min, \tag{2.14}$$

which is a "nonlinear least-squares problem." Most methods for solving (2.14) are based on the quadratic approximation

$$\|r(\alpha)\|^2 \approx \|r(\alpha^{(k)})\|^2 + \langle g(\alpha^{(k)}), \alpha - \alpha^{(k)} \rangle + \tfrac{1}{2} \langle B_k(\alpha - \alpha^{(k)}), \alpha - \alpha^{(k)} \rangle \tag{2.15}$$

of the objection function in the current iteration point $\alpha^{(k)}$. Here, $g(\alpha^{(k)})$ is the gradient of $\|r(\alpha^{(k)})\|^2$, i.e.,

$$g(\alpha^{(k)}) = 2F_k r(\alpha^{(k)}) \tag{2.16}$$

with the matrix F_k given by

$$F_k := ((\nabla r_{i_l})(\alpha^{(k)}), \ldots, (\nabla r_{i_u})(\alpha^{(k)})). \tag{2.17}$$

The concrete methods differ by the choice of B_k, which is thought of as some approximation of the Hessian of $\|r(\alpha^{(k)})\|^2$; see below.

From (2.15), the search direction for the next iterate is obtained by minimizing the right-hand side of (2.15); the first-order necessary condition for this minimum leads to the linear system

$$B_k \gamma^{(k)} = -g(\alpha^{(k)}) \tag{2.18}$$

for the search direction $\gamma^{(k)}$. The next iterate is the defined by

$$\alpha^{(k+1)} := \alpha^{(k)} + \lambda_k \gamma^{(k)}, \tag{2.19}$$

where λ_k is determined by a line search (see below). Note that this approach makes sense only as long as B_k is positive definite, since only then (2.18) is actually sufficient for a minimum in the right-hand side of (2.15), so that $\gamma^{(k)}$ is a descent direction (see, e.g., [20]).

The following choices for B_k are used:

1. Method of steepest descent. $B_k = I$ (although (2.15) is not a good motivation here).

2. Newton's method. Here,

$$B_k := H(\alpha^{(k)}), \tag{2.20}$$

where $H(\alpha)$ is the Hessian of $\|r(\alpha)\|^2$, i.e., $H(\alpha)_{ij} := (\partial^2/\partial\alpha_i\, \partial\alpha_j)(\|r(\alpha)\|^2)$. See (2.32) for an explicit representation.

3. Gauß–Newton method. Here

$$B_k := 2F_k F_k^t, \tag{2.21}$$

where F_k is given by (2.17).

4. Levenberg–Marquardt method. With appropriately chosen parameters γ_k, which especially guarantee that $\gamma^{(k)}$ is a descent direction, B_k is replaced by $B_k + \gamma_k I$ in (2.18).

5. Quasi-Newton method. Here, $B^{(k+1)}$ is calculated from B^k by "update-formulas" in such a way that the "quasi-Newton condition"

$$g^{(k+1)} - g^k = B^{(k+1)}[\alpha^{(k+1)} - \alpha^k] \tag{2.22}$$

is fulfilled. The motivation for (2.22) is as follows: If B^k is close to the Hessian $H(\alpha^k)$, then a Taylor expansion shows that (2.22) holds approximately with $B^{(k)}$ instead of $B^{(k+1)}$; however, since $\alpha^{(k+1)}$ and $g^{(k+1)}$ depend on $B^{(k)}$, this condition would not be manageable, so that one replaces $B^{(k)}$ by $B^{(k+1)}$, which yields (2.22). In concrete quasi-Newton methods, the update formulas are such that (2.22) is fulfilled by updating $B^{(k)}$ by a matrix of rank 1 or 2. In this way, the fast convergence of Newton's method is nearly retained with (in general) much less numerical effort. We use the "Broyden–Fletcher–Goldfarb–Shanno" update formula, which is the following rank-2 update:

$$\begin{aligned} B_{\mathrm{BFGS}}^{(k+1)} := B^{(k)} &+ \frac{1}{\langle \delta^{(k)}, \gamma^{(k)} \rangle} \cdot \Phi^{(k)} \\ &- \frac{1}{\langle \delta^{(k)}, B^{(k)} \delta^{(k)} \rangle} \cdot B^{(k)} \psi^{(k)} B^{(k)}, \end{aligned} \tag{2.23}$$

where

$$\begin{aligned} \phi^{(k)} &:= g(\alpha^{(k+1)}) - g(\alpha^{(k)}) \\ \delta^{(k)} &:= \alpha^{(k+1)} - \alpha^{(k)}, \end{aligned} \tag{2.24}$$

and where the matrices $\Phi^{(k)}$ and $\psi^{(k)}$ are the following dyadic products:

$$\begin{aligned} \Phi_{ij}^{(k)} &:= \phi_i^{(k)} \cdot \phi_j^{(k)}, \\ \psi_{ij}^{(k)} &:= \delta_i^{(k)} \delta_j^{(k)}. \end{aligned} \tag{2.25}$$

We refer to (2.23)–(2.25) as "BFGS-method" below. For other update formulas see [20, pp. 38ff].

After these general discussions concerning the choice of the search direction, a few words concerning the line search are in order, which is used to determine λ_k in (2.19). Usually, the choice of a specific line search algorithm is crucial for the cost and performance of the whole algorithm. There is always a trade-off between cost and accuracy of a line search: "Exact line search," where λ_k is taken as the minimizer of the function $\lambda \to \|r(\alpha^{(k)} + \lambda \gamma^{(k)})\|^2$, is of course costly. See [20] for various "inexact line search strategies." The strategy we use is (S2) from [4] (with initial steplength given by (42) there).

Now we turn to describing our complete algorithm. First, we tried the "hybrid approach" described in [22] as "Method HY2"; this method is a combination of the Gauß–Newton and the BFGS-methods, where the latter is used if there was no sufficient relative reduction of the objective functional in the preceding step. For a problem (2.14), where the minimal value of the objective functional is non-zero (as in our problem), this method tends to yield BFGS-steps towards the end.

This method did not work well for our problem: The matrices $B^{(k)}$ appearing in the Gauß–Newton steps were very ill-conditioned, which resulted in "bad" search directions every time the algorithm chose Gauß–Newton steps. A heuristic reason for the ill-conditioning of $F_k F_k'$ (cf. (2.21)) is the following:

Substituting (2.2), (2.4), and (2.8) into (2.13) gives

$$r_m(\alpha) = \sqrt{w_m}\left(\hat{h}_m - \sum_{i=1}^{n} (\alpha_0 + \tilde{\alpha}_i^2) \cdot \frac{h}{2} \sum_{j=1}^{m-1} c_{mj} \cdot e^{-(t_m - t_j)/\tau_i}\right) \tag{2.26}$$

with suitable coefficients c_{kj}. Hence,

$$\frac{\partial r_m}{\partial \alpha_i}(\alpha) = -2\sqrt{w_m}\,\tilde{\alpha}_i \cdot \left[\frac{h}{2} \sum_{j=1}^{m-1} c_{mj} e^{-(t_m - t_j)/\tau_i}\right]. \tag{2.27}$$

Hence, for any vector $(\beta_1, ..., \beta_n)^t$,

$$(F_k' \beta)_m = -2\sqrt{w_m} \sum_{j=1}^{m-1} c_{mj} \left[\frac{h}{2} \sum_{i=1}^{n} \tilde{\alpha}_i \beta_i e^{-(t_m - t_j)/\tau_i}\right]. \tag{2.28}$$

If $\mathcal{L}$ denotes the Laplace transform of a function β, then it follows from a simple change of variables that

$$\int_0^\infty \beta(\tau) e^{-t/\tau}\, d\tau = \mathcal{L}(\tilde{\beta})(t) \tag{2.29}$$

with

$$\tilde{\beta}(s) := s^{-2} \cdot \beta\left(\frac{1}{s}\right). \tag{2.30}$$

Hence, a comparison of the bracketed term in (2.28) with (2.29) shows that the matrix F_k' acts like a discrete version of a Laplace transform (followed by a convolution with the function -1). Since inverting the Laplace transform is a severely ill-posed problem (cf. Section 4), it is to be expected from the outset that F_k is very ill-conditioned, which actually showed in our computations.

The main idea is now to replace Gauß–Newton steps by Newton steps in the hybrid method HY2 of [22]. In general, Newton steps are very expensive to compute. Here, however, the Hessian is very easy to compute:

It follows from (2.26) that for $l \neq i$, $(\partial^2 r_m / \partial\alpha_l \, \partial\alpha_i)(\alpha) = 0$ and that

$$\frac{\partial^2 r_m}{\partial \alpha_i^2}(\alpha) = \frac{1}{\tilde{\alpha}_i} \cdot \frac{\partial r_m}{\partial \alpha_i}(\alpha). \tag{2.31}$$

Hence, the Hessian $H(\alpha^{(k)})$ of $\|r(\alpha^{(k)})\|^2$ is obtained by differentiating (2.16)–(2.17) using (2.31). This results in

$$H(\alpha^{(k)}) = 2F_k F_k^t + D_k \tag{2.32}$$

with

$$D_k = \operatorname{diag}\left(\frac{[F_k \cdot r(\alpha^{(k)})]_i}{\tilde{\alpha}_i^k}\right). \tag{2.33}$$

Since $F_k F_k^t$ is positive semi-definite, $H(\alpha^{(k)})$ will be positive definite as soon as all diagonal elements d_i of D_k are positive; the smallest eigenvalue is at least $\min_i d_i$.

Since, as mentioned above, F_k can be interpreted as a discretization (via the trapezoidal rule, which has only positive weights) of a Laplace transform followed by a (discretized) convolution with $-l$, we obtain

PROPOSITION 2.2. *If for all* $j \in \{i_l, ..., i_u\}$, $r_j(\alpha^{(k)}) < 0$, *then all diagonal elements of* D_k *are positive.*

To see this, note that l is positive and that the $\tilde{\alpha}_i^{(k)}$ in (2.33) cancel against those in (2.27).

We conclude the following from Proposition 2.2:

1. If all $r_j(\alpha^{(k)})$ are negative, i.e., if the actual parameter vector $\alpha^{(k)}$ "overestimates" the $\hat{h}_i$, then $H(\alpha^{(k)})$ is positive definite and will likely be well-conditioned.

2. If most of the $r_j(\alpha^{(k)})$ are negative, then it is still quite likely that $(\alpha^{(k)})$ is well-conditioned.

3. If most $r_j(\alpha^{(k)})$ are positive, i.e., if the current parameters underestimate most of the $\hat{h}_i$, then $H(\alpha^{(k)})$ will most likely not be positive definite, so that a Newton step will not yield a descent direction.

Note that without the substitution (2.4), the corresponding least-squares problem is a quadratic minimization problem. However, its Hessian is ill-conditioned, as can be seen with the same arguments as those used above for showing that F_k is ill-conditioned. Thus, the transformation (2.4) does not only remove the constraint (2.3), but also has a tendency to make Newton steps more stable at least as long as most of the residuals are negative. These conditions lead to our algorithm:

ALGORITHM 2.3. 1. For an initial guess $\alpha^{(0)}$, let

$$B_0 := H(\alpha^{(0)})$$

be defined by (2.32). If B_0 is not positive definite, replace it by

$$B_0 + vI$$

with $v > 0$ such that $B_0 + vI$ is positive definite. Let $k := 0$ and go to 2.

2. Solve (2.18) for $\gamma^{(k)}$ and define $\alpha^{(k+1)}$ by (2.19) with λ_k determined by the strategy (S2) described in [4] (with initial steplength given by (42) there). With a given $\varepsilon \in]0, 1[$ (we used $\varepsilon = 0.2$), check if

$$\|r(\alpha^{(k)})\|^2 - \|r(\alpha^{(k+1)})\|^2 < \varepsilon \cdot \|r(\alpha^{(k)})\|^2 \tag{2.34}$$

holds. If yes, go to 3.

Otherwise, compute $H(\alpha^{(k+1)})$ as in (2.32). If $H(\alpha^{(k+1)})$ is positive definite, then go to 2 with $B^{(k+1)} := H(\alpha^{(k+1)})$ and k replaced by $k+1$. Otherwise, go to 3.

3. Compute $B^{(k+1)}$ via (2.23) and go to 2 with k replaced by $k+1$.

This algorithm is performed until (2.34) holds for $\varepsilon = 0.01$ five times in a row. This stopping criterion, which says that five iterations in a row yields less than 1%

very well (also for negative α_0 in (2.3)). The number of iterations typically needed for $n = 20$ up to $n = 70$ degrees of freedom, $i_{\max} = 256$ or 512, was between 10 and 20. The final value for $\chi^2/(i_u - i_l + 1)$ (with χ^2 defined by (2.10)) was always between 0.9 and 1.2. We support these claims by reporting about one of these tests in the next section.

3. NUMERICAL EXAMPLES I

In the following examples, predetermined amplitude distributions were inserted into (1.2) (in the discrete form (2.2) with $n = 1000$). The resulting functions were convolved with the lamp function l shown by broken lines in Fig. 3.1.1. Then, Gaussian noise (with variance equalling the function value) was added. The resulting values were taken as data $\hat{h}_i$ and are shown as dots in Fig. 3.1.1 for Example 3.1. The solid line in this figure shows the resulting reconvolution $I(t_i, \tilde{f})$, where $\tilde{f}$ is determined via (2.2) and (2.4) from the parameters $\alpha = (\tilde{\alpha}_1, ..., \tilde{\alpha}_n)$ generated by Algorithm 2.3. This figure also shows the scaled residuals $r(\alpha)$ (see (2.13)) and their autocorrelation. (Because of space considerations, the corresponding figures for the other examples are not shown here, but are available in a preprint version of this paper from the authors.) The piecewise linear interpolation of the resulting values for the "amplitudes" $(\tilde{a}_1, ..., \tilde{a}_n)$ is shown in Figs. 3.1.2, 3.2, 3.3, 3.4, and 3.5.

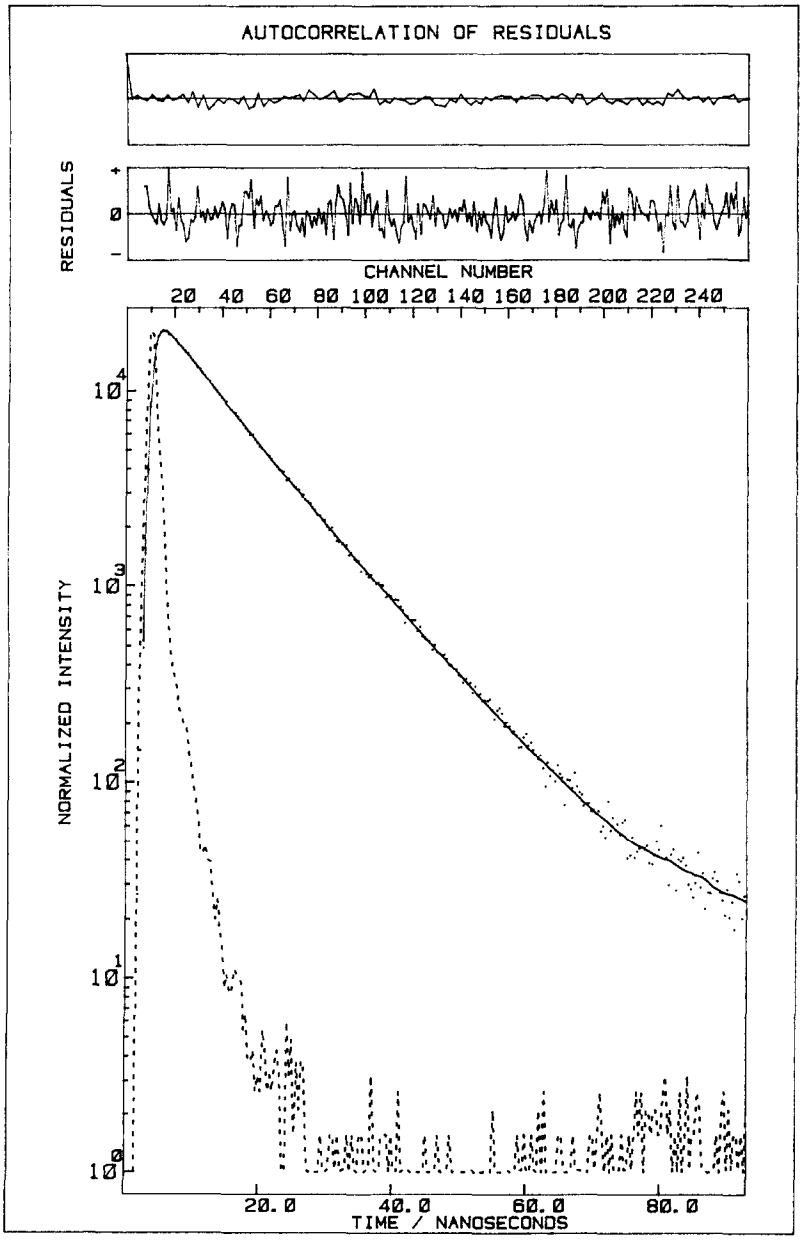
AUTOCORRELATION OF RESIDUALS
RESIDUALS
+
Ø
-
CHANNEL NUMBER
20 40 60 80 100 120 140 160 180 200 220 240
NORMALIZED INTENSITY
10^4
10^3
10^2
10^1
10^Ø
20.Ø
40.Ø
60.Ø
80.Ø
TIME / NANOSECONDS

FIGURE 3.1.1

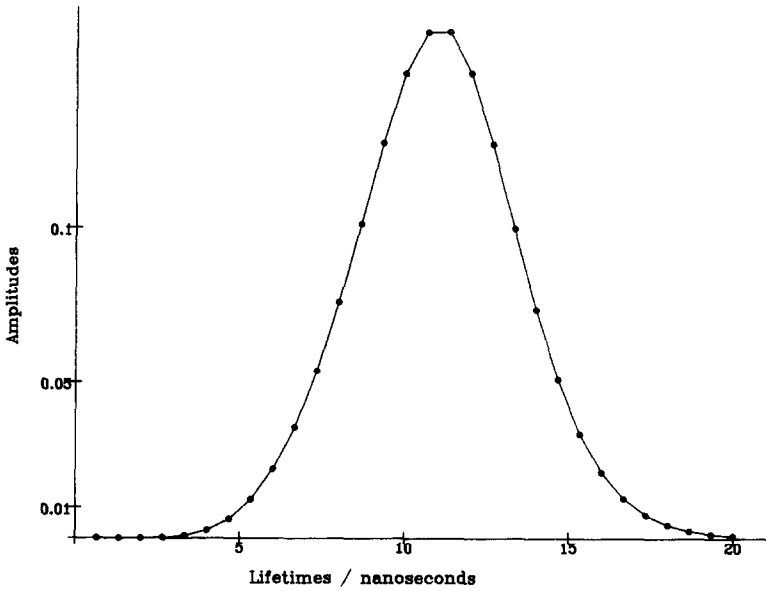

FIGURE 3.1.2

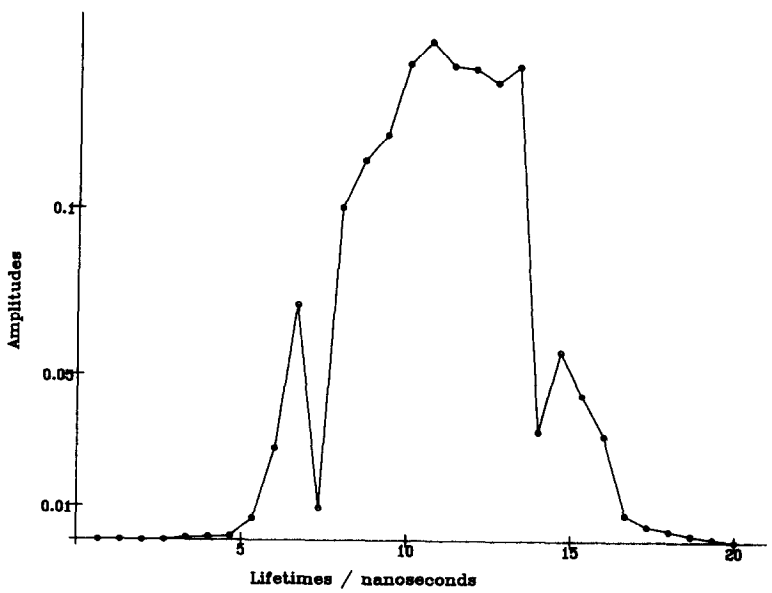

FIGURE 3.1.3

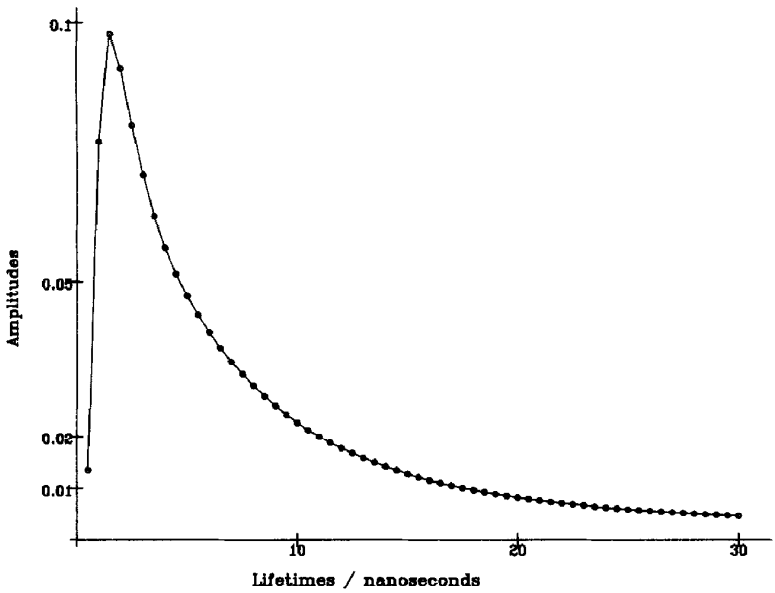

FIGURE 3.2

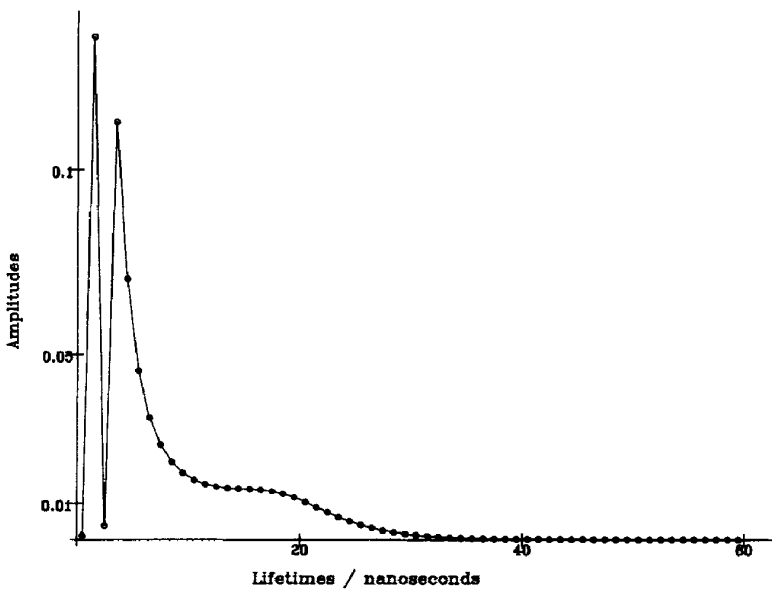

FIGURE 3.3

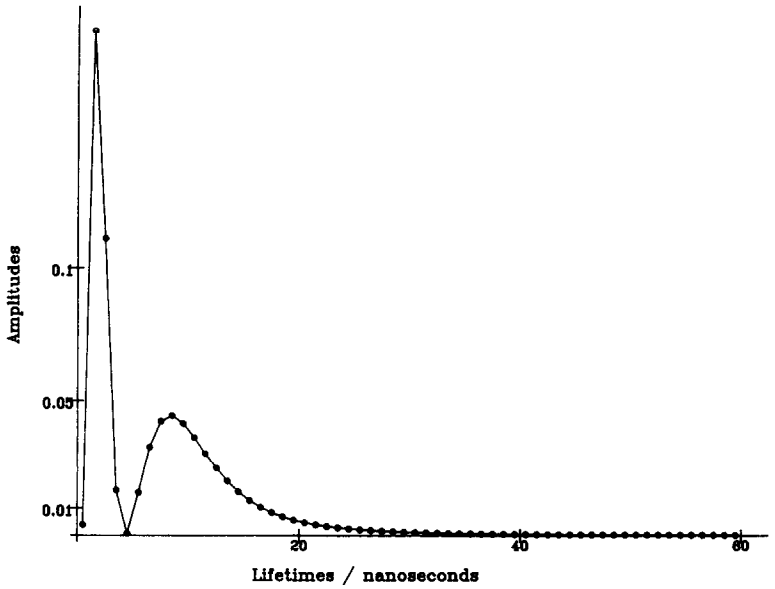

FIGURE 3.4

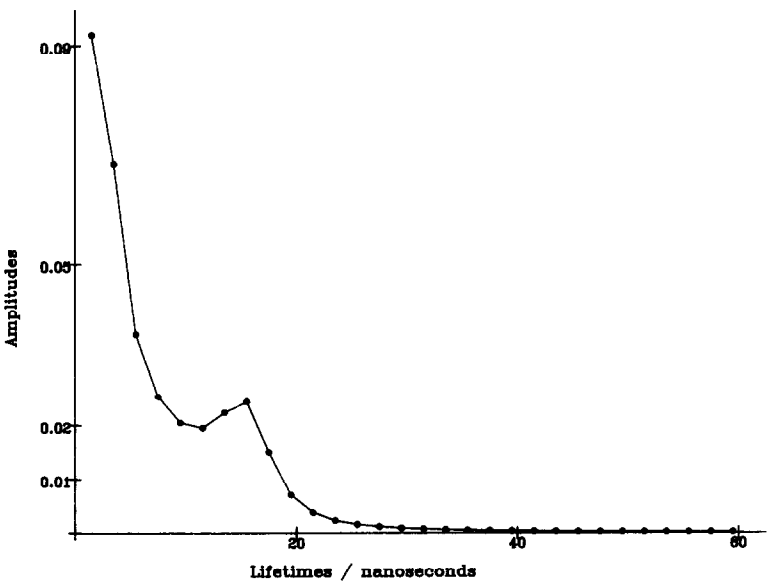

FIGURE 3.5

EXAMPLE 3.1. The predetermined amplitude distribution was Gaussian with the maximum at $\tau = 10$. We took $n = 30$, $i_l = 7$, $i_u = 256$, and obtained $\chi^2/250 = 1.02$ after 12 iterations of Algorithm 2.3. The results are shown in Figs. 3.1.1 (in logarithmic scale) and 3.1.2. The reconstruction is quite satisfactory. Note that our algorithm is designed to reconstruct $\tilde{f}$ and, not directly, the underlying amplitude distribution. Since the link between those two is a Laplace transform whose inversion is ill-posed, we think that the reconstruction in this example is pretty good.

We now show by an example that in Algorithm 2.3, it was essential to combine Newton steps and quasi-Newton steps. Figure 3.1.3 shows the reconstructed amplitude distribution from the data of Example 3.1 if only Newton steps are used. Compared to Fig. 3.1.2, the result is much worse. The reason for this seems to be that while Algorithm 2.3 forces $B^{(k)}$ to stay positive definite all the time, this is not the case if only Newton steps are used (cf. the discussion following Proposition 2.2).

The following examples serve the purpose to show the limitations of the approach of Section 2 and to motivate the development to be outlined in Section 4. They are generated in the same way as Example 3.1. As predetermined amplitude distribution, the function $\alpha(t) = C \cdot t^{-3/2} \cdot e^{-\sigma/t^2}$ was chosen (cf. [11]). We made a lot of comparative computations which differ from each other by noise level, the number of degrees of freedom, and the location of the τ_i (cf. (2.2)). We report about some of the results in Table I. These examples show the following effects: α can be reconstructed well with moderate noise if the points τ_i are concentrated in the part of the τ-axis where the function α actually varies (Example 3.2). With the same n, the reconstruction is much worse even for low noise if the τ_i vary in a larger interval. Examples 3.4 and 3.5 show that in the presence of noise, increasing the number of degrees of freedom makes the reconstruction worse.

The reason for this strange behavior, which we observed also in other examples, lies in the ill-posedness of our problem. This will be explained in the next section.

4. ILL-POSEDNESS AND REGULARIZATION

Recall Hadamard's definition of a well-posed problem: A problem is called "well-posed," if for all admissiable data, a solution exists and the solution is unique and

TABLE I

Example	Noise	n	$\tau_i \in \cdots$	Reconstructed amplitudes contained in Fig.
3.2	Moderate	60	[0.5, 30]	3.2
3.3	Low	60	[0.5, 60]	3.3
3.4	High	60	[0.5, 60]	3.4
3.5	High	30	[1.5, 60]	3.5

depends continuously on the data (in a topology which makes sense for the concrete problem). If any of these requirements is violated, then the problem is called "ill-posed." Ill-posed problems, especially those, where the solution depends discontinuously on the data, pose serious numerical problems: "Naive" algorithms not taking the ill-posedness into account will be numerically unstable; i.e., even small data errors will have catastrophic effects. For a general survey about various aspects of ill-posed problems and methods for their numerical treatment see [5, 17, 24, 26, 49]. As can be seen, e.g., from [24], integral equations of the first kind are "nearly always" (in a precise sense) ill-posed. Note that both (2.1) and (1.2) are integral equations of the first kind (of convolution type).

One of the most severly ill-posed problems is the problem of inverting the Laplace transform. Thus, the closely related integral equation (1.2) is severely ill-posed: Even small noise in f may lead to large perturbations in α. Now in our problem, also f is related to the actually measured function h via (2.1), which is again an ill-posed problem. It can be concluded form [27] that if h and l are continuous and strictly increasing in a neighborhood of 0, then f is uniquely determined by (2.1). This equation can be written as an operator equation

$$Kf = h \tag{4.1}$$

on a suitable Hilbert, e.g., an L^2, space, where

$$(Kf)(t) := \int_0^t l(t-s)\, f(s)\, ds \tag{4.2}$$

is a (non-selfadjoint) compact operator with L^2-adjoint

$$(K^*u)(\sigma) = \int_\sigma^T l(t-\sigma)\, u(t)\, dt, \tag{4.3}$$

if l has its support in $[0, T]$.

Under the conditions mentioned above that guarantee the unique solvability of (2.1), the kernel (null-space) $N(K) = \{0\}$, so that 0 is not an eigenvalue of K. However, since 0 is always an element of the spectrum of this compact operator, 0 is in its essential spectrum. Thus, $R(K)$ is at most dense in L^2 and K^{-1}, defined on $R(K)$, is everywhere discontinuous. This shows that (2.1) is really ill-posed as an equation between L^2-spaces (and similarly, between all reasonable function spaces) in the sense that a solution does not always exist and that the solution, if it exists, depends discontinuously on the data h.

When discretizing an ill-posed problem, the approximating system of linear equations become more and more ill-conditioned as their dimensions increase (see, e.g., [14, 15]); "coarse discretization" regularizes a problem, while this regularization becomes weaker as the discretization becomes finer. Since the Ansatz (2.2) can be seen as a discretization, this explains the behaviour, see in Examples 3.4 and 3.5:

Increasing the number of degrees of freedom makes the approximating problem more ill-conditioned, so that the data error is propagated more seriously into the solution f. Thus, using an even higher degree of freedom will not make the result better, but worse.

Our approach can either be seen as solving (2.1) via the discretization (2.2), or, [illegible] bining this with a discretization for (2.2). We think that it is precisely the roughness of the approximation of the integral operator in (1.2) that enables our Algorithm 2.3 to produce reasonable results even for the amplitude distributions. If one tries to use a better approximation (instead of (2.2)) for the integral operator in (1.2), then the ill-posedness of (1.2) will be felt more strongly and the results will get worse if nothing is done to counteract this.

Methods for dealing with ill-posed problems are called "regularization methods"; besides "regularization by discretization," which is what we have done, the method of "Tikhonov regularization" is used. For (4.1), this method reads as follows: If instead of h, one has perturbated data h_δ with $\|h-h_\delta\| \leqslant \delta$, the "regularized solution" x_μ^δ is defined via

$$\|Kf-h_\delta\|^2+\mu\,\|Lf\|^2 \to \min \tag{4.4}$$

or, equivalently,

$$(K^*K+\mu L^*L)f=K^*h_\delta, \tag{4.5}$$

where $\mu>0$ is the "regularization parameter" and L is a suitable linear operator; e.g., $L=I$ or L is a differential operator like $Lf=f^{(k)}$. The choice of $\mu=\mu(\delta)$ is crucial for convergence with $\delta\to 0$, for stability and for convergence rates; it can be thought of as a trade-off between accuracy (μ small) and stability (μ large). See, e.g., [16 and the references quoted there] for the choice of μ. In practical computations, (4.4) or (4.5) have to be combined with discretization.

Note that under reasonable assumptions, the regularized solutions and their discretized versions converge to the "true solution" as the noise level and the regularization parameter tend to 0 in a synchronized way. Thus, the following regularized version of Algorithm 2.3, motivated by (4.4), can be expected to yield approximations to the decay function f and can therefore be considered as a "deconvolution" of (2.1). In contrast, Algorithm 2.3 should be seen as a "reconvolution algorithm" in the sense that it produces approximations that make the functional in (2.10) small without guaranteeing that these approximations actually converge to the true decay function.

ALGORITHM 4.1. Use Algorithm 2.3 (with the obvious changes) for minimizing

$$\|r(\alpha)\|^2+\mu\,\|D^2\alpha\|^2 \tag{4.6}$$

instead of $\|r(\alpha)\|^2$. Here, $D^2\alpha$ is the following difference quotient approximating the second derivative,

$$(D^2\alpha)_i := \frac{\tilde{\alpha}_{i+1} - 2\tilde{\alpha}_i + \tilde{\alpha}_{i-1}}{K^2}, \qquad i \in \{1, ..., n\}, \tag{4.7}$$

where $\tilde{\alpha}_0 = \tilde{\alpha}_{n+1} := 0$ and the τ_i were assumed to be equally spaced such that $\tau_i = \tau_0 + iK$. $\mu > 0$ is a fixed regularization parameter.

The "obvious changes" in Algorithm 4.1 concern the concrete form of the gradient and the Hessian of (4.6), which can be computed easily from the corresponding quantities in Algorithm 2.3.

Algorithm 4.1 can be thought of as a discrete version of (4.4). The additional term $\mu \|D^2\alpha\|^2$ penalizes oszillations in α. In the next section, we report about some numerical examples obtained with Algorithm 4.1.

5. Numerical Examples II

The following example is similar to Example 3.1:

Example 5.1. A predetermined Gaussian amplitude distribution with maximum at $\tau = 14.5$ was used as in Example 3.1 (with moderate noise) to generate data; however, while in Example 3.1, the data were generated via (2.2) with $n = 1000$, we used only $n = 10$ here, so that the data are not too good. Then we used Algorithm 4.1 (always with $n = 30°$ of freedom) first with $\mu = 0$ (which is just Algorithm 2.3) and then with two non-zero values of the regularization parameter with the results shown in Table II.

Even a closer look at the residuals did not reveal significant differences. It is obvious that regularization improves the reconstruction considerably. The regularization parameter, which is usually thought of as "small," is up to 10^4 here. However, this is only a question of scaling.

TABLE II

μ	Reconstructed amplitudes contained in Fig.
0	5.1.1
1000	5.1.2
10,000	5.1.3

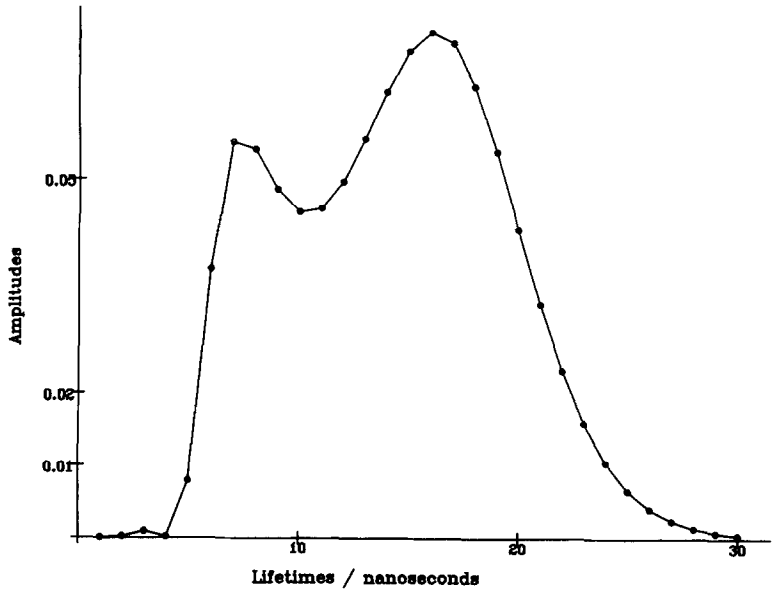

FIGURE 5.1.1

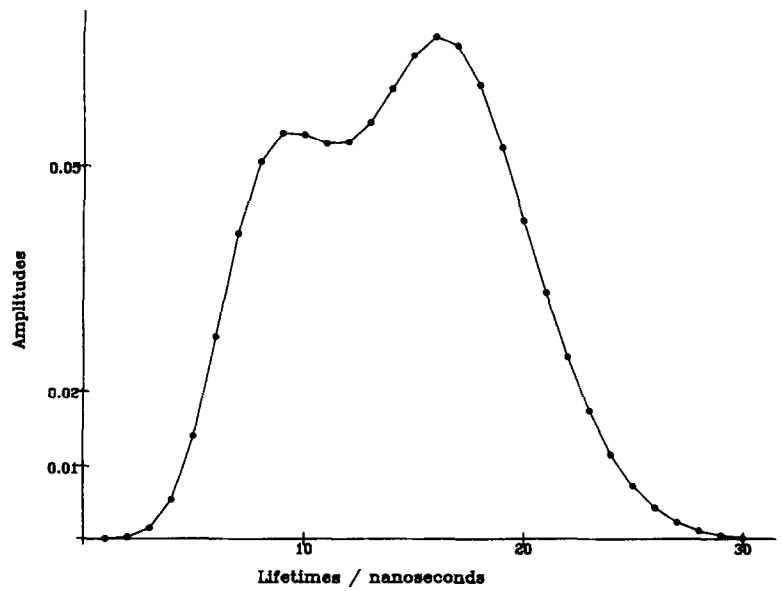

FIGURE 5.1.2

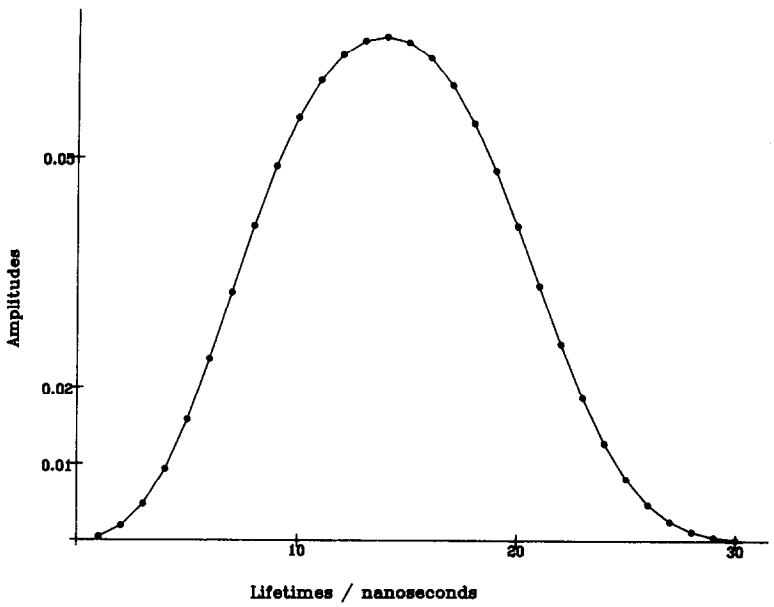

FIGURE 5.1.3

EXAMPLE 5.2. The data are the same as in Example 3.3, where the reconstruction was quite bad. We used the same $n(=60)$ and τ_i as in Example 3.3 and obtained the results shown in Table III with Algorithm 4.1.

A comparison of Figs. 5.2.1, 5.2.2, 5.2.3, and 3.3 (which corresponds to $\mu=0$) shows the effect of regularization. For $\mu=10^5$, the reconstruction looks as it should. For all these values of μ, the residuals are roughly uniform. However, the value for $\chi^2/(i_u-i_e+1)$ increases from 0.91 for $\mu=50$ to 1.45 for $\mu=10^5$, which reflects the trade-off between accuracy and stability mentioned above.

EXAMPLE 5.3. Here, we analyze the excimer fluorescence of poly-(1-vinyl) naphthalene [33]. Figure 5.3.1 shows the decay fluorescence pattern (convolved

TABLE III

μ	Reconstructed amplitudes contained in Fig.
50	5.2.1
100	5.2.2
100,000	5.2.3

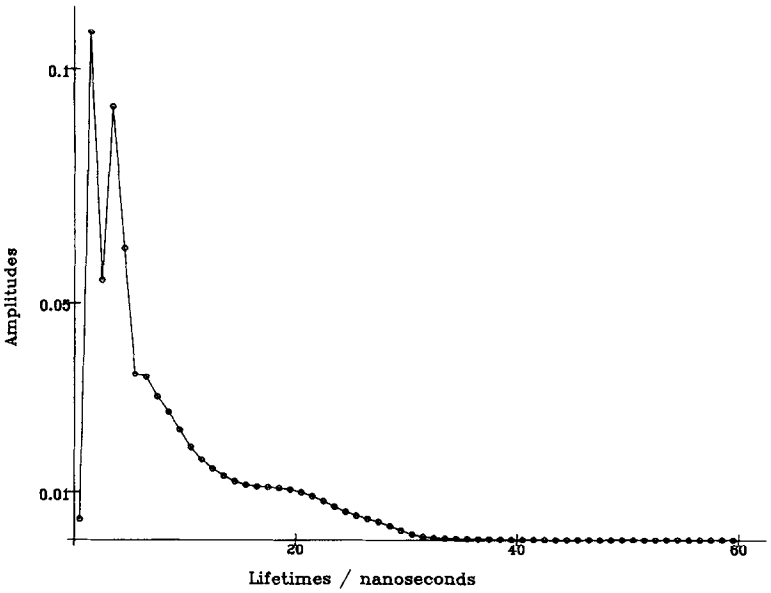

FIGURE 5.2.1

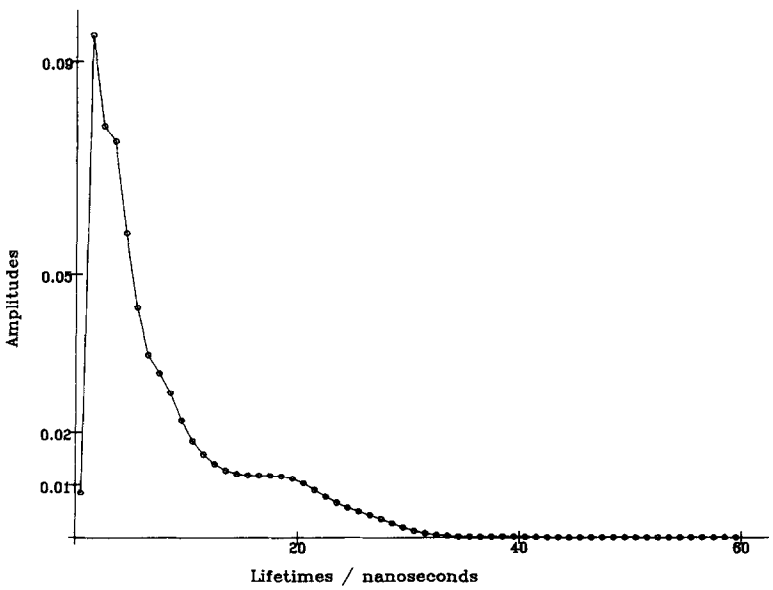

FIGURE 5.2.2

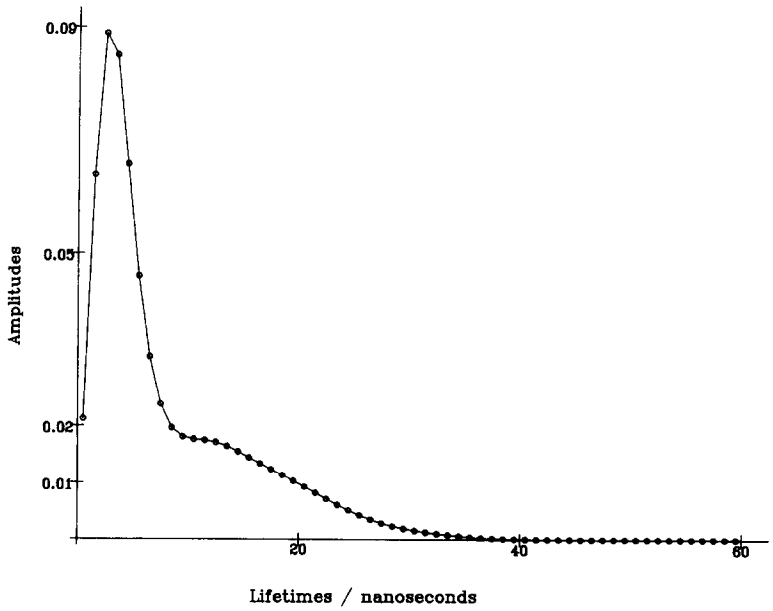

FIGURE 5.2.3

with the lamp function; $\lambda_{em} = 480$ mm, $\lambda_{exc} = 313$ nm) and the fit obtained with Algorithm 2.3; for the fit, we used $n = 25$ with exponentially distributed values for the τ_i, $i_l = 19$, $i_u = 256$, and obtained $\chi^2/238 = 1.10$. The reconstructed amplitudes are shown (in logarithmic scale) in Fig. 5.3.2. Distributions of negative amplitudes are centered around 0.5 and 15 ns, respectively, resulting in the typical rise of excimer formation (see Fig. 5.3.1). While Algorithm 2.3 clearly reconstructs these negative amplitudes, it also generates an oscillation between 2 and 7 ns. With Algorithm 4.1 (with $\mu = 10$), these oscillations are damped as shown in Fig. 5.3.3 ($\chi^2/238 = 1.14$). These results do not allow us to distinguish between a distribution or a discrete set of lifetimes; for this, the experimental data ($2 * 10^4$ counts in peak maximum) in our experiment are not good enough: More accurate transient data with CPM values above 10^5 would be required to allow more definite decisions on the basis of statistical criteria.

These results show that regularization is certainly a promising approach for our problem. However, more work has to be done, e.g., concerning an automatic choice of the regularization parameter as suggested in [16].

While Algorithm 4.1 is a modification of Algorithm 2.3 that incorporates Tikhonov regularization, we also constructed a similar modification for the maximum entropy method (cf. [47]). The numerical results were comparable to those obtained with Algorithm 4.1.

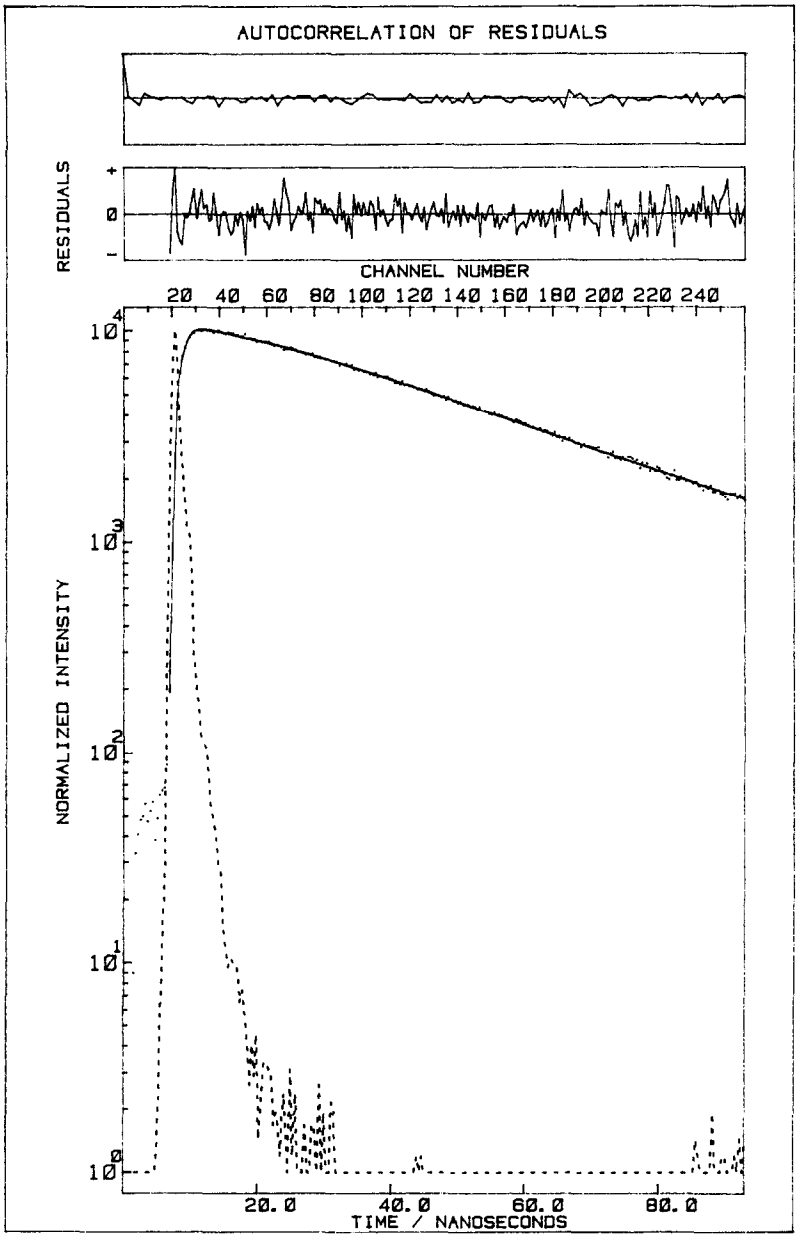
AUTOCORRELATION OF RESIDUALS
RESIDUALS
+
0
-
CHANNEL NUMBER
20 40 60 80 100 120 140 160 180 200 220 240
NORMALIZED INTENSITY
10^4
10^3
10^2
10^1
10^0
20.0
40.0
60.0
80.0
TIME / NANOSECONDS

FIGURE 5.3.1

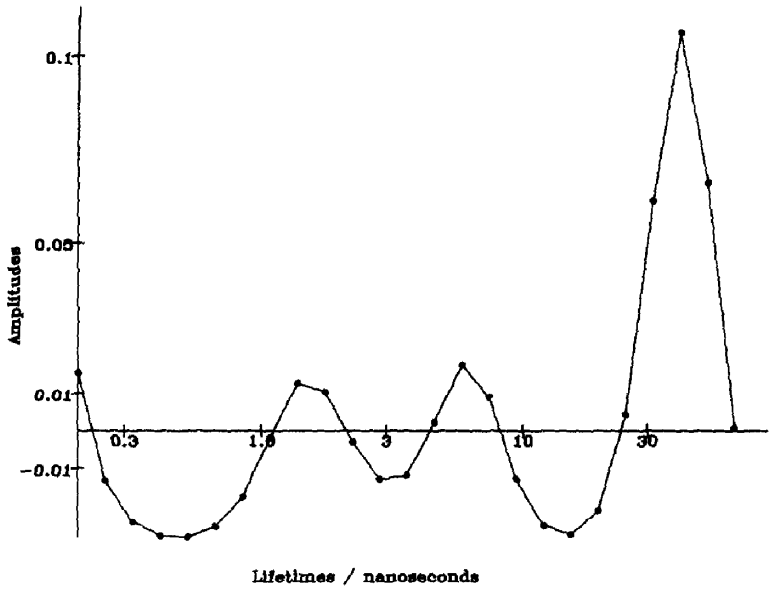

FIGURE 5.3.2

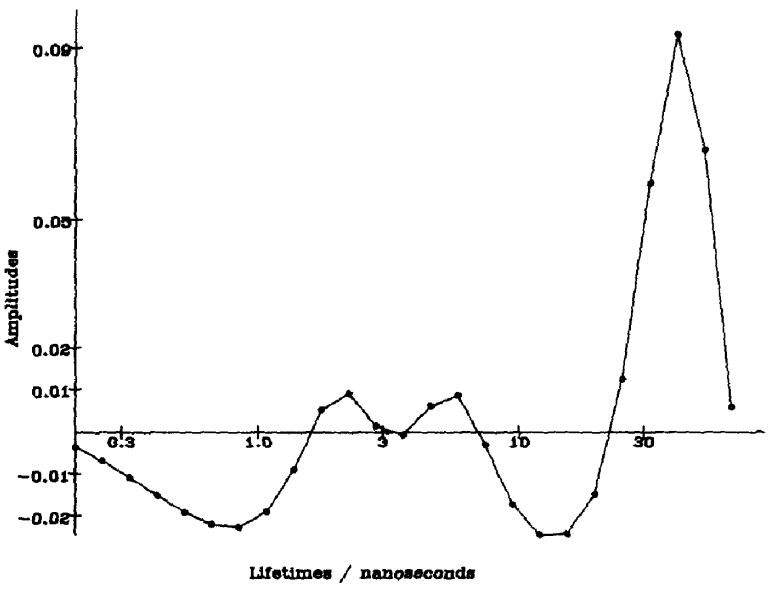

FIGURE 5.3.3

REFERENCES

1. P. A. ANFINRUD, D. E. HART, J. F. HEDSTROM, AND W. S. STRUVE, *J. Phys. Chem.* **90**, 2374 (1986).
2. V. M. AGRANOVICH AND R. M. HOCHSTRASSER, (Eds.), *Spectroscopy and Excitation Dynamics of Condensed Molecular Systems* (North-Holland, Amsterdam, 1983).
3. V. M. AGRANOVICH AND M. D. GALANIN, *Electronic Excitation Energy Transfer in Condensed Matter* (North-Holland, Amsterdam, 1982).
4. M. AL-BAALI AND R. FLETCHER, *J. Opt. Theor. Appl.* **48**, 359 (1986).
5. J. BAUMEISTER, *Stable Solution of Inverse Problems* (Vieweg, Braunschweig, 1987).
6. J. B. BIRKS, D. J. DYSON, AND I. H. MUNRO, *Proc. Roy. Soc. London Ser. A* **275**, 575 (1963).
7. J. B. BIRKS, *Photophysics of Aromatic Molecules* (Wiley, London/New York, 1970), p. 301.
8. N. BOENS, M. AMELOOT, I. YAMAZAKI, AND F. C. DE SCHRYVER, *Chem. Phys.* **121**, 73 (1987).
9. M. BOUCHY (Ed.), *Deconvolution and Reconvolution of Analytical Signals, Applications to Fluorescence Spectroscopy* (ENSIC-INPL, Nancy, 1983).
10. E. M. BUCHBERGER, B. MOLLAY, W.-D. WEIXELBAUMER, H. F. KAUFFMANN, AND W. KLÖPFFER, *J. Chem. Phys.* **89**, 635 (1988).
11. A. CARASSO, *SIAM. J. Appl. Math.* **47**, 892 (1987).
12. R. B. CUNDALL AND R. E. DALE (Eds.), *Time-Resolved Fluorescence Spectroscopy in Biochemistry and Biology*, NATO-ASI Series A: Life Sciences, Vol. 69 (Plenum, New York, 1983).
13. F. C. DE SCHRYVER, P. COLLART, J. VANDENRIESSCHE, R. GOEDEWEEK, A. SWINNEN, AND M. VAN DER AUWERAER, *Acc. Chem. Res.* **20**, 159 (1987).
14. H. W. ENGL, *Boll. Geodes. Sci. Aff.* **41**, 291 (1982).
15. H. W. ENGL, "On the Convergence of Regularization Methods for Ill-Posed Linear Operator Equations," in *Improperly Posed Problems and Their Numerical Treatment*, edited by G. Hämmerlin and K.-H. Hoffmann (Birkhäuser, Basel, 1983), p. 81.
16. H. W. ENGL AND H. GFRERER, *Appl. Numer. Math.* **4**, 395 (1988).
17. H. W. ENGL AND C. W. GROETSCH (Eds.), *Inverse and Ill-Posed Problems* (Academic Press, Orlando, FL, 1987).
18. U. EVEN, K. RADEMAN, J. JORTNER, N. MANOR, AND R. REISFELD, *Phys. Rev. Lett.* **52**, 2164 (1984).
19. G. R. FLEMING, *Chemical Applications of Ultrafast Spectroscopy* (Oxford Univ. Press, London, 1986).
20. R. FLETCHER, *Practical Methods of Optimization. Vol* 1. *Unconstrained Optimization* (Wiley, Chichester, 1980).
21. R. FLETCHER, *Practical Methods of Optimization. Vol.* 2. *Constrained Optimization* (Wiley, Chichester, 1981).
22. R. FLETCHER AND C. XU, *IMA J. Numer. Anal.* **7**, 371 (1987).
23. A. GRINVALD AND I. STEINBERG, *Anal. Biochem.* **59**, 583 (1974).
24. C. W. GROETSCH, *The Theory of Tikhonov Regularization for Fredholm Equations of the First Kind* (Pitman, Boston, 1984).
25. D. E. HART, P. A. ANFINRUD, AND W. S. STRUVE, *J. Chem. Phys.* **85**, 2689 (1987).
26. B. HOFMANN, *Regularization for Applied Inverse and Ill-Posed Problems* (Teubner, Leipzig, 1986).
27. B. HOFMANN, *Z. Anal. Anw.* **7**, 247 (1988).
28. C. E. HOYLE AND J. M. TORKELSON (Eds.), *Photophysics of Polymers*, Symposium Series, Vol. 358 (ACS, Washington, DC, 1987).
29. D. JAMES AND W. R. WARE, *Chem. Phys. Lett.* **120**, 455 (1985).
30. D. JAMES AND W. R. WARE, *Chem. Phys. Lett.* **126**, 7 (1986).
31. D. JAMES AND W. R. WARE, *Chem. Phys. Lett.* **138**, 181 (1987).
32. D. JAMES AND W. R. WARE, *J. Phys. Chem.* **89**, 5450 (1985).
33. H. F. KAUFFMANN, W. D. WEIXELBAUMER, J. BÜRBAUMER, AND B. MOLLAY, "Electronic Energy Relaxation in Aromativ Vinyl Homopolymers," in [28, p. 220].
34. J. KLAFTER AND A. BLUMEN, *J. Chem. Phys.* **80**, 875 (1984).
35. J. KLAFTER AND A. BLUMEN, *Chem. Phys. Lett.* **119**, 377 (1985).

36. J. KLAFTER AND M. F. SHLESINGER, *Proc. Natl. Acad. Sci. USA* **83**, 848 (1986).
37. P. LIANOS AND S. MODES, *J. Phys. Chem.* **91**, 6088 (1987).
38. A. D. LIVESEY AND J. C. BROCHON, *Biophys. J.* **52**, 693 (1987).
39. B. MOLLAY, G. LANDL, AND H. F. KAUFFMANN, *J. Chem. Phys.* **91**, 3744 (1989).
40. D. V. O'CONNOR AND D. PHILLIPS, *Time-Correlated Single Photon Counting* (Academic Press, London, 1984).
41. D. V. O'CONNOR, W. R. WARE, AND J. C. ANDRÉ, *J. Phys. Chem.* **83**, 1333 (1979).
42. K. A. PETERSON AND M. D. FAYER, *J. Chem. Phys.* **85**, 4702 (1985).
43. K. A. PETERSON, M. B. ZIMT, S. LINSE, R. P. DOMINGUE, AND M. D. FAYER, *Macromolecules* **20**, 168 (1987).
44. D. PINES AND D. HUPPERT, *J. Chem. Phys.* **89**, 1177 (1988).
45. R. D. ROSENKRANTZ (Ed.), *Papers on Probability, Statistics and Statistical Physics by E. T. Jaynes* (Reidel, Dordrecht, 1983).
46. A. SIEMARCZUK AND W. R. WARE, *J. Phys. Chem.* **91**, 3677 (1987).
47. C. R. SMITH AND W. T. GRANDY, JR. (Eds.), *Maximum-Entropy and Bayesian Methods in Inverse Problems* (Reidel, Dordrecht, 1985).
48. A. SZABO (Ed.), *Excited State Probes in Biochemistry and Biology*, NATO-ASI Series (Plenum, New York, 1987).
49. A. TIKHONOV AND V. ARSENIN, *Solutions of Ill-Posed Problems* (transl. from the Russian) (Wiley, New York, 1977).
50. M. VINCENT, J.-C. BROCHON, F. MEROLA, W. JORDI, AND J. GALLAY, *Biochemistry* **27**, 8752 (1988).
51. B. WAGNER, D. R. JAMES, AND W. R. WARE, *Chem. Phys. Lett.* **138**, 181 (1987).
52. W. R. WARE, "Techniques in Pulse Fluorometry," in [12, p. 23].
53. G. WILLIAMS AND D. C. WATTS, *Trans. Faraday Soc.* **66**, 80 (1970).
54. M. A. WINNIK (Ed.), *Photophysical and Photochemical Tools in Polymer Sciences: Conformation, Dynamics, Morphology*, NATO-ASI Series, C: Mathematical and Physical Sciences, Vol. 182 (Reidel, Dordrecht, 1986).
55. M. VAN DEN ZEGEL, N. BOENS, D. DAEMS, AND F. C. DE SCHRYVER, *Chem. Phys.* **101**, 311 (1986).
56. M. ZUKER, A. G. SZABO, L. BRAMALL, D. T. KRAJCARSKI, AND B. SELINGER, *Rev. Sci. Instrum.* **56**, 14 (1985).